Molecular Crystals and Liquid Crystals

ISSN: 1542-1406 (Print) 1563-5287 (Online) Journal homepage: http://www.tandfonline.com/loi/gmcl20

Spectroscopic and Quantum Chemical Studies of (Z)-N'-(3-(hidroksiimino)butan-2-ylidene)-4-metilbenzensulfonohidrazide Ligand

Feyizan Güntepe, Murat Çinarli, Canan Kazak & Hümeyra Bati

To cite this article: Feyizan Güntepe, Murat Çinarli, Canan Kazak & Hümeyra Bati (2015) Spectroscopic and Quantum Chemical Studies of (Z)-N'-(3-(hidroksiimino)butan-2-ylidene)-4-metilbenzensulfonohidrazide Ligand, Molecular Crystals and Liquid Crystals, 616:1, 213-225, DOI: 10.1080/15421406.2014.991135

To link to this article: http://dx.doi.org/10.1080/15421406.2014.991135

Mol. Crys. and Liq. Crys., Vol. 616: pp. 213–225, 2015

ISSN: 1542-1406 print/1563-5287 online
DOI: 10.1080/15421406.2014.991135

Spectroscopic and Quantum Chemical Studies of (Z)-*N′*-(3-(hidroksiimino)butan-2-ylidene)-4-metilbenzensulfonohidrazide Ligand

FEYIZAN GÜNTEPE,[1,*] MURAT ÇINARLI,[2] CANAN KAZAK,[1] AND HÜMEYRA BATI[2]

[1]Department of Physics, Faculty of Arts and Sciences, Ondokuzmayis University, Samsun, Turkey
[2]Department of Chemistry, Faculty of Arts and Sciences, Ondokuzmayis University, Samsun, Turkey

The structural and spectroscopic characterization of Schiff base ligand, (Z)-N′-(3-(hidroksiimino)butan-2-ylidene)-4metilbenzensulfonohidrazide (HL) are presented in this paper. The optimized geometry and vibrational frequencies of the ligand have been calculated by using DFT/B3LYP method with 6-311G(d,p) and 6-311G+(d,p) basis sets. The calculated wave numbers are used to assign vibrational bands obtained in IR spectroscopy and find out to the manifestations of hydrogen bonding in the ν_{str}(N–H) and ν_{str}(O–H) vibrations. The UV-Vis absorption peaks of the ligand predicted by the time-dependent DFT method matched quite well with experimentally observed UV-Vis bands. The molecular electrostatic potential and the energy profile with respect to rotations about the selected torsion angle τ(C5-S1-N3-N2) is also calculated.

Keywords Crystal structure; DFT calculation; IR spectra; oxime; sulfonyl hydrazone

Introduction

Over the years, oximes have been widely used as very efficient complexing agent in analytical chemistry for isolation, separation, and extraction of different metal ions [1–6]. Oxime derivatives are very important compounds because of their biological activity, such as insecticidal, miticidal, nematocidal activities, antidote activities for organophosphor poison [7]. Some oxime and hydrazone complexes was found to be active as antibacterial, antitubercular antilepral, antimalarial, and certain kinds of tumors [8–12]. Metal complexes of oxime serve as models biosystems such as vitamin B_{12} and miyocardial perfusion imaging agents [13]. Hydrazones and their metal complexes also possess pronounced biological and pharmaceutical activities, as antitumor [14, 15], antimicrobial [16], antitubercilosis [17], and antimalarial agents [18]. Hydrazones play an important role in improving the

*Address correspondence to Feyizan Güntepe, Department of Physics, Faculty of Arts and Sciences, Ondokuz Mayis University TR-55139, Kurupelit, Samsun/Turkey. E-mail: feyizanguntepe@gmail.com

Color versions of one or more of the figures in the article can be found online at www.tandfonline.com/gmcl.

antitumor selectivity and toxicity profile of antitumor agents by forming drug carrier system employing suitable carrier proteins [19]. Specifically sulfonly hydrazones have been shown to be active in several pharmacological tests, demonstrating antibacterial, diuretic, antiviral, antinociceptive activity, specific enzyme inhibition such as carbonic anhydrase, γ-secratese HIV-protease, metalloproteinase and hormone regulation among others [20–22]. Sulfonyl hydrazides grafted onto the nanoparticles are also used as polymerizable foaming agent [23]. The hydrazones are also important for their use as plasticizers and stabilizers for polymers [24], polymerization initiators, and antioxsidant [25]. Hydrazones possessing an azomethine −NH−N=CH− proton constituent an important class of compounds for new drug development. Therefore, many researchers have synthesized these compounds as target structures and evaluated their biological activities [26]. Besides, the compound is a model for studies on vibrational spectra in hydrogen bonding system. Vibrational spectra provide the most commonly used criteria for the presence and properties of hydrogen bonds. The most significant spectral changes resulting from H-bond formation occur in the IR spectra in the region of X-H stretching bands. These are the decrease in frequency in the N-H stretching mode, increase of its intensity, broadening of the bands, and appearance of a complex fine structure [27]. The mechanism of this phenomenon is subject of many theoretical studies. On the other hand, alternative computational methods have long been carried out for equilibrium structure properties of molecular system such as geometry, vibrational frequency, absorption spectrum, etc. Computational methods are also widely used for simulating IR spectra [28]. Such simulations are indispensable tools to perform normal mode analysis so that modern vibrational spectroscopy is unimaginable without involving them. In this study, the ligand is characterized spectroscopically and theoretically. Herein, we present a comparative analysis of DFT calculations with experimental ones.

Methods

Melting point (Mp) was determined by Electrothermal 9100 melting point apparatus. The oxime-sulfonylhydrazone Schiff base ligand (HL) was synthesized according to procedure reported in literature [29] (Mp: 181 (°C) % Yield: 72). The FT-IR spectrum was recorded in KBr pellet using an ATI Unicam-Mattson 1000 FT-infrared spectrometer 4000–400 cm^{-1} range. The absorption spectra of the ligand were performed on a Unicam UV-2-100 spectrometer in methanol solvent.

All the calculations are performed for the ligand by using Gaussian 03 program package on a personal computer [30]. The molecular structure of the ligand in the ground state (in vacou) was optimized using Becke's three-parameter hybrid exchange functional (B3) [31, 32] in combination with correlation functional of Lee Yang and Parr (LYP) [33] were employed in the DFT calculations. Two different basis sets were used the 6-311G(d,p); valance triple zeta plus polarization functions of d and p type and the 6-311G+(d,p); valance triple zeta plus diffuse function and polarization functions of d and p type. For modeling, the initial guess of ligand was obtained from the X-ray refinement data. The harmonic vibrational frequencies analysis was performed at the same level of theory. At the optimized structure of the molecule no imaginary frequency modes were obtained, providing that a true minimum on the potential energy surface was found. The electronic transitions for the molecule were calculated using time-dependent DFT method. The most widely used ab initio approach in UV-visible calculations is the time-dependent density functional theory which for a reasonable computational effort, commonly yields to accurate results, especially when hybrid functional are used [34]. The molecular electrostatic potential (MEP) map and

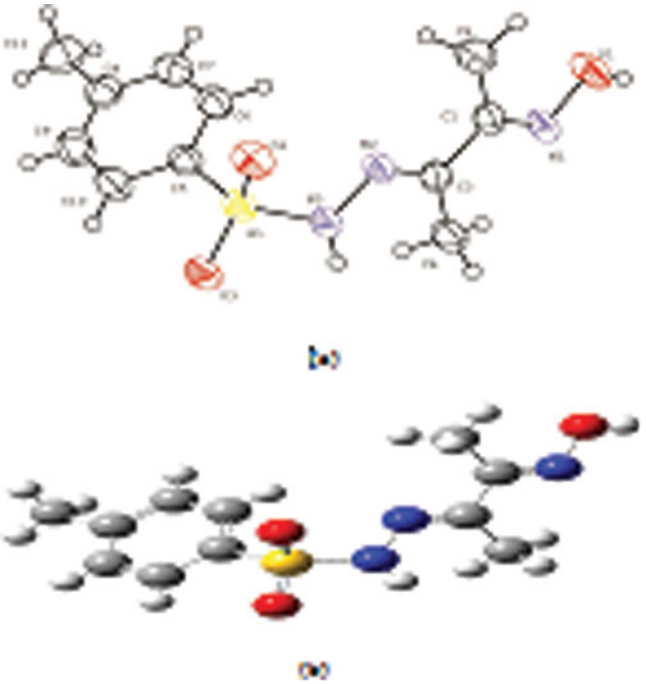

Figure 1. (a) ORTEP drawing of the basic crystallographic unit of the title compound, showing the atom-numbering scheme. Displacement ellipsoids are drawn at the 40% probability level and all H atoms are shown as small spheres of arbitrary radii. (b) The optimized geometry computed with the B3LYP/6–311G+(d, p) level.

frontier molecular orbital surfaces are visualized by GausView Molecular Visualization program [35].

Result and Discussion

Optimized Structures

The crystal structure of ligand was determined by X-ray diffractions method by Bolhosa et al. [29]. The title compound is shown in Fig. 1 (a) as an Ortep III view with the optimized geometry computed with the B3LYP/6–311G+(d,p) level in Fig. 1 (b). In order to verify the accuracy of used theoretical model the investigated molecule is fully optimized in the gas phase and optimized geometries are compared with experimental geometry in literature [29]. Some selected bond lengths, bond angles, and torsion angles calculated by B3LYP/6-311G(d,p) and B3LYP/6-311G+(d,p) level are listed in Table 1 with experimental ones.

As can be seen in Table 1 most of the calculated bond lengths are slightly longer than the experimental ones. It was noted that the experimental results belong to solid phase and theoretical calculations belong to gaseous phase. In the solid state, the existence of the crystal field along with the intermolecular interactions have connected the molecules together, which result in the differences of geometric parameters between the calculated and experimental values. The largest difference between experimental and calculated bond

Table 1. Selected experimental and optimized geometric parameters of the title compound

		DFT/B3LYP	
Parameters	Experimental [29]	6-311G(d,p)	6-311G+(d,p)
Bond lengths (Å)			
C1-N1	1.272(3)	1.286	1.286
C5-C6	1.381(3)	1.393	1.392
C5-C10	1.384(3)	1.392	1.394
C6-C7	1.374(3)	1.389	1.391
C7-C8	1.381(3)	1.400	1.399
C8-C9	1.379(4)	1.398	1.401
C9-C10	1.373(4)	1.391	1.390
C1-C3	1.481(3)	1.478	1.479
C1-C2	1.491(3)	1.501	1.501
C3-N2	1.279(3)	1.288	1.288
C3-C4	1.492(3)	1.506	1.506
C5-S1	1.754(2)	1.792	1.793
N1-O1	1.403(2)	1.396	1.399
N2-N3	1.386(2)	1.359	1.361
N3-S1	1.632(18)	1.709	1.713
O2-S1	1.418(15)	1.450	1.452
O3-S1	1.432(15)	1.457	1.459
RMSE[a]		0.0272	0.0282
Max. difference[a]		0.077	0.081
Bond angles (°)			
N1-C1-C3	115.61(19)	115.531	115.382
N1-C1-C2	124.9(2)	123.452	123.482
C3-C1-C2	119.4(2)	121.015	121.134
N2-C3-C1	114.21(19)	116.063	115.894
N2-C3-C4	125.7(2)	123.592	123.538
C1-C3-C4	120.04(19)	120.341	120.564
C1-N1-O1	112.93(18)	111.745	111.718
C3-N2-N3	117.81(17)	118.247	118.185
N2-N3-S1	116.54(14)	116.923	116.732
O2-S1-O3	119.94(10)	123.205	122.861
O2-S1-N3	107.87(9)	107.249	107.164
O3-S1-N3	104.18(9)	102.312	102.282
O2-S1-C5	108.54(10)	108.164	108.128
O3-S1-C5	108.01(10)	108.648	108.769
N3-S1-C5	107.69(10)	105.945	106.454

(Continued on next page)

Table 1. Selected experimental and optimized geometric parameters of the title compound *(Continued)*

		DFT/B3LYP	
Parameters	Experimental [29]	6-311G(d,p)	6-311G+(d,p)
RMSE[a]		1.524	1.449
Max. difference[a]		3.265	2.921
Dihedral angles (°)			
N1-C1-C3-N2	−179.9(2)	−177.640	−177.417
C2-C1-C3-N2	−0.2(3)	2.248	2.548
N1-C1-C3-C4	0.0(3)	2.824	3.174
C2-C1-C3-C4	179.7(2)	−177.286	−176.859
C3-C1-N1-O1	−179.69(18)	179.419	179.590
C2-C1-N1-O1	0.6(3)	−0.466	−0.374
C1-C3-N2-N3	−178.00(18)	−178.421	−178.310
C4-C3-N2-N3	2.1(3)	1.096	1.078
C3-N2-N3-S1	−166.64(17)	−167.771	−166.900
N2-N3-S1-O2	−40.74(19)	−54.433	−56.497
N2-N3-S1-O3	−169.23(15)	174.669	173.078
N2-N3-S1-C5	76.23(18)	60.919	59.019
C10-C5-S1-O3	13.6(2)	−18.836	−20.897
C6-C5-S1-O2	60.0(2)	25.991	23.862

[a]RMSE and maximum differences between the bond lengths and the bond angles computed by the theoretical method and those obtained from X-ray diffraction.

length is 0.0339 Å which is calculated with 6-311G+(d,p) basis set for N3−S1. The largest difference between experimental and calculated bond angle is 5.588° which is calculated with B3LYP/6-311G+(d,p) for O3−S1−N3. The largest differences are caused by intermolecular hydrogen bonds due to charge redistribution in this part of molecule. The mentioned intermolecular hydrogen bonds are reported in literature [29] like that: the crystal structure is stabilized by a combination of intermolecular N−H . . . O (N3−H8 . . . O3^{i}) and O−H . . . N (O1−H1 . . . N1^{ii}) hydrogen bonds. (Symmetry codes: (i)-*x*+2, -*y*, -*z*; and (ii) -*x*, -*y*+1, -*z*.). It is generally recognized that for an accurate description of hydrogen bonds system at least double zeta quality basis augmented with a set of polarization and diffuse functions set is needed [36]. Therefore, a somewhat better geometry description is expected with 6-311G+(d,p) basis set. Using the root mean square (RMS) error for consideration it is found that the both basis sets provide the same RMS value of 0.0141 Å for bond lengths while the B3LYP/6-311G+(d,p) calculation provide the lowest RMS value of 2.040° for bond angles. Consequently, the B3LYP calculations with both basis sets predict very closer geometry so the basis sets used in calculations have no significant effect on the results. It is noted that the calculated N−H, O−H bond length cannot be compared with experimental one, as X-ray diffraction technique does not locate properly hydrogen atoms, especially in hydrogen bonded systems [37].

Vibrational Spectra

The FT-IR spectrum of the ligand is shown in Fig 2. Based on optimized geometries harmonic vibrational frequencies were calculated by using same method and basis sets as. The

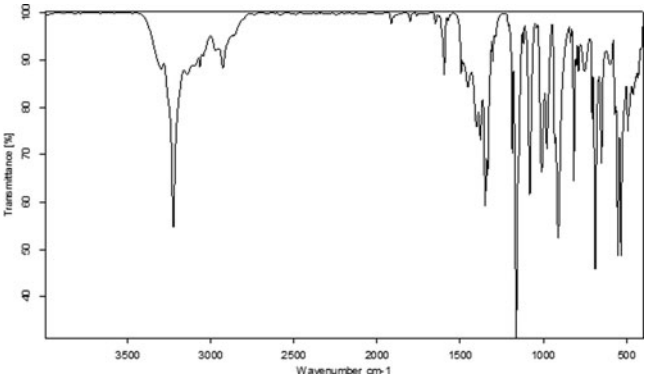

Figure 2. The experimental FT-IR spectrum of the title compound.

calculated frequencies were not scaled. Frequency calculations at the same level of theory revealed no imaginary frequencies indicating that an optimal geometry at these levels of approximation was found for the ligand. By using Gauss View molecular visualization program [35], the vibrational band assignments have been made. The experimental and calculated frequencies are given in Table 2 with their assignments. It is well known that the calculated "nonscale" harmonic frequencies could significantly overestimate experimental values due to lack of electron correlation, insufficient basis sets and anharmonicity, and the experimental results belong to solid phase and theoretical calculations belong to gaseous phase. Thus, there is a reasonable agreement between experimental and calculated frequencies, except for the O−H and N−H stretching bands. The band observed at 3298 cm^{-1} is attributed to the absorption of the ν(NH) stretching vibration of hydrazone which is calculated 3479 and 3471 cm^{-1} for 6-311G(d,p) and 6-311+G(d,p) respectively. The ν(OH) stretching vibration of oxime is observed at 3226 cm^{-1} which is calculated as 3835 and 3831 cm^{-1} for 6-311G(d,p) and 6-311+G(d,p), respectively. As mentioned above, one of the spectral changes in IR spectrum resulting from H-bond formation is the decrease in frequency in the X-H stretching mode. Both the hydrazone and oxime group have hydrogen bonding capability as much as stronger than alcohol, phenol, and carboxylic acid groups [38]. So such differences between experimental and calculated frequencies for ν(OH) and ν(NH) bands could be expected for the modes in a medium strong hydrogen bond [39]. For substituted benzenes, the ν(CH) stretching modes are expected in the region of 3105–3000 cm^{-1} [40]. In the present study, the bands observed at 3144, 3100, and 3068 cm^{-1} are attributed to aromatic ν(CH) stretching vibrations and were calculated using B3LYP/6-311G(d,p) and B3LYP/6-311+G(d,p) 3213/3201/3170 and 3210/3199/3167 cm^{-1}, respectively. The strong band at 1597 is assigned to ν(C=N) stretching of oxime and hydrazone. This band was computed as 1653 and 1646 cm^{-1} for B3LYP/6-311G(d,p) and B3LYP/6-311+G(d,p), respectively. The band centered at 1340 cm^{-1} is assigned as ν(S=O) stretching and computed as 1322 and 1312 cm^{-1} for B3LYP/6-311G(d,p) and B3LYP/6-311+G(d,p), respectively. The band centered at 1080 cm^{-1} is assigned as ν(N−O) stretching and computed as 1040 and 1035 cm^{-1} for B3LYP/6-311G(d,p) and B3LYP/6-311+G(d,p), respectively. These values are in accord with those of previously reported oximes and hydrazones [41–43]. Since our main interest of IR study is the characterization of hydrogen bonds no elaborate normal mode analysis was performed and only the approximate description of selected modes is given in Table 2.

Table 2. Comparison of the observed and calculated vibrational frequencies (cm^{-1}) of the title compound

		DFT/B3LYP (cm^{-1})	
Assignments	Experimental (cm^{-1})	6-311G(d,p)	6-311G+(d,p)
υ_{str} (NH) hydrazine	3298	3479	3471
υ_{str} (OH) oxim	3226	3835	3831
$\upsilon_{sym\text{-}str}$ (CH) aromatic	3144	3213	3210
$\upsilon_{sym\text{-}str}$ (CH) aromatic	3100	3201	3199
$\upsilon_{asym\text{-}str}$ (CH) aromatic	3068	3170	3167
$\upsilon_{asym\text{-}str}$ (CH_3)	2974	3168	3160
$\upsilon_{sym\text{-}str}$ (CH_3)	2929	3028	3026
υ_{str} (C=N) oxime + υ_{bend} (OH) oxime	1649	1676	1670
υ_{str} (C=N)hydrazine	1597	1653	1646
υ_{str} (CC) aromatic	1490	1638	1635
υ_{sci} (CH_3)	1454	1493	1491
υ_{bend} (NH)	1402	1423	1421
υ_{bend} (NH) + υ_{bend} (OH)	1378	1393	1390
υ_{str} (CC) aromatic + υ_{bend} (CH) aromatic	1347	1329	1329
$\upsilon_{asym\text{-}str}$ (S=O) + υ_{bend} (NH) + υ_{bend}(OH)	1340	1322	1312
υ_{str} (CC) aromatic	1184	1229	1228
$\upsilon_{sym\text{-}str}$ (S=O)	1163	1132	1126
υ_{str} (CC) aromatic + υ_{str} (NO)	910	956	951
$\upsilon_{bend\text{-}out\ of\ plane}$ (CH)	750	853	852
$\upsilon_{bend\text{-}out\ of\ plane}$ (CC)	686	713	723
$\upsilon_{bend\text{-}out\ of\ plane}$ (OH) + $\upsilon_{bend\text{-}out\ of\ plane}$ (NH)	649	607	637

Vibrational modes: str; stretching, bend; bending, sci; scissoring, sym; symmetric, asym; asymmetric.

Molecular Electrostatic Potential

The MEP is a very useful descriptor for determining sites of chemical reactivity of the molecule for electrophilic attack and nucleophilic reactions as well as hydrogen-bonding interactions [39, 44, 45]. To predict reactive sites for electrophilic and nucleophilic attack of the molecule, MEP was calculated at the B3LYP/6–311G+(d,p) optimized geometry and shown in Fig. 3. The negative (red) regions of MEP were related to electrophilic reactivity and the positive (blue) regions related to nucleophilic reactivity. It can be seen from Fig. 3, there are two possible sites on the ligand for electrophilic attack with a maximum value of -0.057 a.u. and -0.054 a.u which around electronegative O atoms. However, positive (blue) regions are localized on hydrogen atoms of oxime and hydrazone moiety. These results provide information about potential hydrogen bond or metal complexing side of molecule. Therefore, Fig. 3 confirms the existence of O–H . . . N and N–H . . . O interactions.

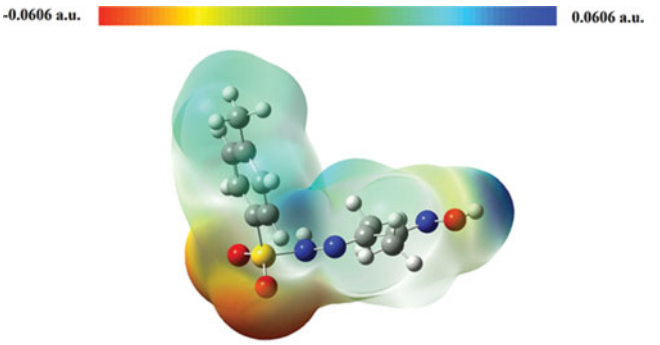

Figure 3. Molecular electrostatic potential map (in a.u.) of the title compound computed with the B3LYP/6–311G+(d, p) level.

Absorption Spectra and Frontier Molecular Orbital Analysis

The absorption spectra of the ligand was recorded in methanol at room temperature and theoretical absorption spectra is predicted by using TD-DFT method based on B3LYP/6-311G+(d,p) level optimized structure. A comparison of calculated (vertical excitations) and experimental electronic spectrum is reported in Fig. 4 and all of the data are listed in Table 3. The visible absorption spectrum of the ligand appears as multiple absorption bands at higher energies (250 and 227 nm). In the calculated spectrum, these bands appear a composition of three excitations at 4.518 eV (λ=274.41 nm, $f = 0.2561$), 4.8783 eV (λ=254.16 nm, $f = 0.1203$), and 5.0380 eV ($\lambda = 246.10$ nm, $f = 0.1680$). As seen from Fig. 4, the three bands appeared in the calculated spectrum having some differences (about 0.15 eV red shifted) compared to the experimental spectrum. The reasons for the discrepancy between the experimental values and theoretical predictions may be as follows: TD-DFT approach is based on the random-phase approximation method [46–48] which provides an alternative to computationally demanding multireference configuration interaction methods in the study

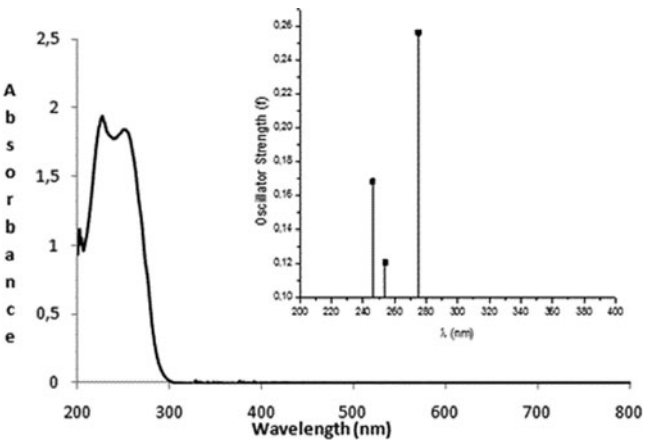

Figure 4. The experimental absorption spectrum of the title compound in methanol solution. Inset: Calculated absorption spectra of title compound. The excited states are shown as vertical bars with high equal to oscillator strength.

Table 3. Experimental and theoretical electronic absorption spectra values

Excitation	Electronic transition	Oscillator strength (f)	λ_{theo} (nm)	λ_{exp} (nm)
1	71(HOMO)→72(LUMO) 71(HOMO)→73(LUMO+1)	0.2561	274.12	250
2	69(HOMO-2)→72(LUMO) 69(HOMO-2)→73(LUMO+1) 70(HOMO-1)→72(LUMO) 71(HOMO)→72(LUMO) 71(HOMO)→73(LUMO+1) 71(HOMO)→74(LUMO+2)	0.1203	254.16	
3	68(HOMO-3)→72(LUMO) 69(HOMO-2)→72(LUMO) 69(HOMO-2)→73(LUMO+1) 70(HOMO-1)→72(LUMO) 70(HOMO-1)→74(LUMO+2) 71(HOMO)→72(LUMO) 71(HOMO)→73(LUMO+1) 71(HOMO)→74(LUMO+2)	0.1680	246.10	227

of excited states. TD-DFT calculations do not evaluate the spin–orbit splitting; the values are averaged. Here, in this paper the objective is to evaluate the electronic structure by direct electronic excitations and only singlet–singlet transitions considered. In addition, the role of solvent effect of solution is not included in the theoretical calculation.

The B3LYP/6-311G+(d,p) calculation indicate that the ligand has 71 occupied MOs. The surface and energy levels of the highest occupied molecular orbital (HOMO), the lowest unoccupied molecular orbital (LUMO), HOMO-1, and LUMO+1 orbitals of the ligand are shown in Fig. 5. The value of energy separation between the HOMO and LUMO is 4.95 eV and this large energy gap indicates that the ligand is quite stable. Analyses of frontier molecular orbital provide helpful information for studies on electrical and optical properties as well as in UV–Vis spectrum and chemical reactions [49]. The maximum absorption of calculated electronic absorption spectrum corresponding to electronic transition from the HOMO to the LUMO. As can be seen from the Fig. 5 while the electrons are delocalized over the hydrazone and oxime fragment in HOMO, they are delocalized among all the atoms in LUMO. These frontier molecular orbitals are mainly composed of p atomic orbitals; therefore, the above electronic transitions are mainly derived from the contribution of the to $\pi \rightarrow \pi^*$ bands.

Conformational Analysis

In order to determine the preferential position of hydrazone moiety with respect to SO_2 group a preliminary search of low-energy structures was performed using AM1 computations as a function of the selected degrees of torsional freedom τ(C5-S1-N3-N2). The calculated energy profile with respect to rotations about the selected torsion angle τ(C5-S1-N3-N2) is given in Fig. 6 with the optimized geometries of the most favorable and unfavorable conformations which is proceed the orientation of hydrazone moiety with

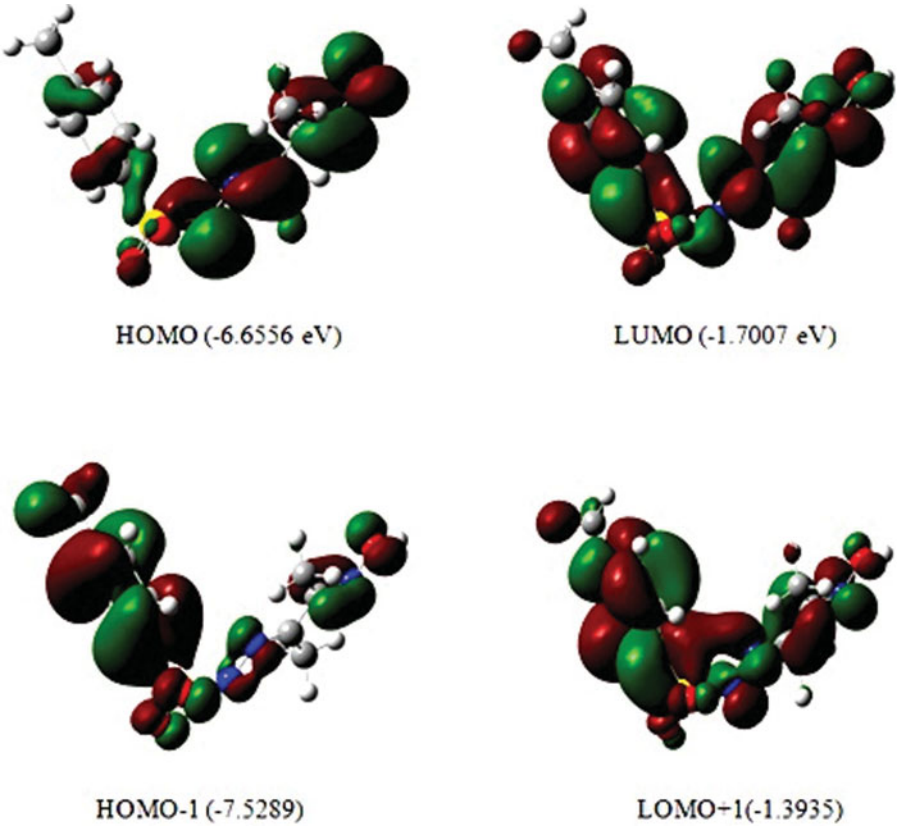

Figure 5. Molecular orbital surfaces and energy levels given in parentheses for the HOMO-1, HOMO, LUMO, LUMO+1 of the title compound computed with the B3LYP/6–311G+(d, p) level.

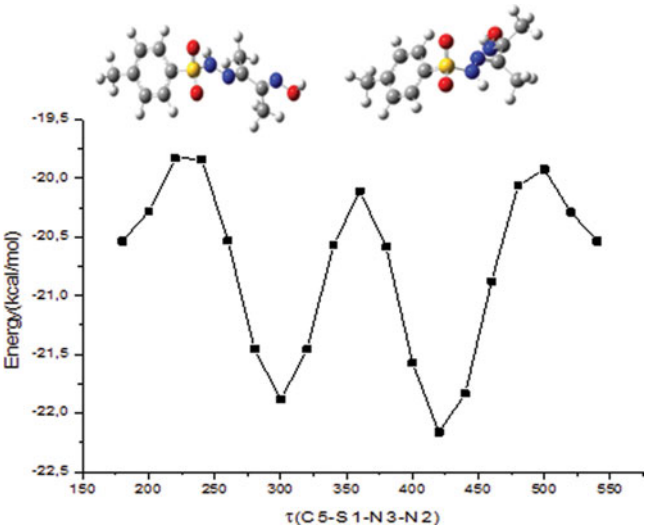

Figure 6. Energy profile of the optimized counterpart of the title compound for the rotation about τ (C5-S1-N3-N2) torsion angle.

respect to SO_2 group. The respective value of the selected degree of torsion angle τ(C5-S1-N3-N2) is 75.70(12)° in literature [29], whereas the corresponding value in optimized geometry is 60.919° for B3LYP/6-311G(d,p) and 59.019° for B3LYP/6-311+G(d,p). As can be seen from Fig. 6, the minimum energy domain is located at 60° having energy of -22.1619 kcal/mol, the maximum energy is also located at 220° having energy of -19.8302 kcal/mol. Energy difference between the most favorable and unfavorable conformer, which arises from rotational potential barrier calculated with respect to the selected torsion angle is calculated as 2.3317 kcal/mol when both selected degrees of torsion angle are considered. The molecular energy can be divided into bonded and nonbonded contributions. The bonded energy is considered to be independent of torsional angle changes and therefore vanished when relative conformer energies are calculated. The nonbonded energy is further separated into torsional steric and electrostatic terms. Hydrogen bond is an intense electrostatic contribution [50]. Owing to the fact that the ligand contains intramolecular hydrogen bonds, the computational results allow us to predict the most stable conformer is principally determined by the nonbonded torsional energy and also electrostatic energy terms affected by packing of the molecules.

Conclusions

In this study, we have characterized the Schiff base ligand (Z)-N'-(3-(hidroksiimino)butan-2-ylidene)-4metilbenzensulfonohidrazide (HL) by spectroscopic and quantum chemical methods.

The optimized geometries compared with the structure obtained by (XRD) technique reported in literature [29]. Take account of the fact that the experimental results belong to solid phase and theoretical calculations belong to gaseous phase, the general agreement is good and calculations support the solid-state structure. The IR spectra supported by DFT calculations was particularly devoted to the manifestations of hydrogen bonding in the ν_{str}(N–H) and ν_{str} (O–H) vibrations. The calculated MEP map agrees well with solid-state interactions. The maximum absorption wavelength of calculated electronic absorption spectrum is comparable with electronic transition from the HOMO to the LUMO. As a result, all of these calculations will be provide helpful information to further studies on the title compound.

References

[1] Chakravorty, A. (1974). *Coord. Chem. Rev.*, *1*, 13.
[2] Chattaopadhyay, S., Ray, M. S., Chaudhuri, S., Mukhopadyay ,G., Bocelli, G., Cantoni, A., & Ghosh, A. (2006). *İnorg. Chim. Acta*, *1367*, 359.
[3] Ray, M. S., Ghosh A., Bhattacharya, R., Mukhopadyay, G., Drew, M. G. B., & Ribas, J. (2004). *J. Chem. Soc.*, Dalton Trans. 252.
[4] Wan, S., Mori, W., Yamada, S., & Murahashi, S. I. (1989). *Bull. Chem .Soc. Jpn.*, *43*, 62.
[5] Kukushkin, V.Yu., Tudela, D., & Pompeiro, A. J. L. (1999). *Coord. Chem. Rev.*, *33*, 156.
[6] Mohanty, G., & Chakravorty, A. (1976). *Inorg. Chem.*, *15*, 2912.
[7] Sevagapandian, S., Rajagopal, G., Nehru, K., & Athappan, P. (2000). *Trans. Met.Chem. 388*, 25.
[8] Hania, M. M. (2009). *E-J. Chem.*, *508* (S1), 6.
[9] Petering, H. G., & Buskik, H. H. (1963). *G.E.Underwood. Cancer Res*., *367*, 64.
[10] Jayaraju, D., & Kondapi, A. K. (2001). *Curr. Sci.*, *787* (7), 81.
[11] Liu, L., Nam, S., Tian, Y., Yang, F., Wu, J., Wang, Y., Scuto, A., Polychronopoulos, P., Magiatis, M., Skaltsounis, L., & Jove, R. (2011). *Cancer Res.*, *3972* (11), 71.

[12] Barybin, M. V., Diaconescu, P. L., & Cummins, C. C. (2001). *İnorg.Chem.*, *2892*, 40.
[13] Dash, S. P., Pasayat, S., H. R., Dash, S., Das, S., Butcher, R. J., & Dinda, R. (2012). *Polyhedron*, *31*, 524.
[14] Kumar, V. K., & Rao, M. R. (2010). *Int. J. Pharma Bio. Sci.*, *1* (2), V1.
[15] Easmon, J., Puerstinger, G., Roth, T., Fiebig, H. H., Jenny, M., Jaeger, W., & Heinisch, G., (2001). *J. Hofm ann, Int. J. Cancer*, *89*, 94.
[16] Vicini, P., Zani, F., Cozzini, P., & Doytchinova, I. (2002). *Eur. J. Med. Chem.*, *553*, 37.
[17] Patole, J., Sandbhor, U., Padhye, S., Deobagkar, D. N., Anson, C. E., & Powell, A. (2003). *Bioorg. Med. Chem. Lett.*, *51*, 13.
[18] Walcourt, A., Loyevsky, M., Lovejoy, D. B., Gordeuk, V. R., & Richardson, D. R. (2004). *Int. J. Biochem. Cell. Biol. 401*, 36.
[19] Kratz, F., Beyer, U., Roth, T., Tarasova, N., Collery, P., Lechenault, F., Cazabat, A., Schumacher, P., Unger, C., & Falken, U. (1998). *J. Pharm. Sci. 338*, 87.
[20] Özbek, N., Alyar, S., & Karacan, N. (2009). *J. Mol. Struct. 48*, 938.
[21] Ozawa, Y., Sugi, N., Nagasu, T., Owa, T., Watanabe, T., Koyanagi N., Yoshino, H., Kitoh, K., & Yoshimathu, K., (2001). *Eur. J. Cancer*, *37*, 2275.
[22] Lima, L. M., Amarante, E. G., Miranda, A. L. P., Faraga, C. A. M., & Barreiro, E. J. (1999). *Pharma. Pharmacol. Commun.*, *5*, 673.
[23] Caj, L. F., Rong, M. Z., Zhang, M. Q., & Ruan, W. H. (2007). *Compos. Mater. Struct.*, *334* (Pts.1 and 2), 729.
[24] Kuehn, U., Warzeska, S., Pritzkow, H., & Kramer, R. J. (2001). *Am. Chem. Soc.*, *123*, 8125.
[25] Karlin, K. D. *et al.* (1983J). *Biochemistry Chemical and Inorganic Perspectives*, Adenine Press, Guilderland: New York.
[26] Gadhawala, Z. M., Harsoliya, M. S., Doi, R. M., Panchbhayya, G. M., & Modasiya, M. K. (2012). *J. Pharm. Res.*, *5*(8), 4113.
[27] Wojcik, M. J., Kwiendacz, J., Boczar, M., Boda, L., & Ozaki, Y. (2010). *Chem. Phy.*, *372*, 72.
[28] Sheeja, S. R., Mangalam, N. A., Kurup, M. R. P., Marry, Y. S., Raju, K., Varghese, H. T., & Panicker, C. Y. (2010). *J. Mol. Struct.*, *973*, 36.
[29] Bulhosa, M. C. S., Gervini, V. C., Bresolin, L., Locatelli A., & Olivera, A. B. (2012). *Acta Cryst. Ev 68*, o592.
[30] Frisch, M. J., Trucks, G. W., Schlegel, H. B., Scuseria, G. E., Robb, M. A., Cheeseman, J. R., Montgomery, Jr., J. A., Vreven, T., Kudin, K. N., Burant, J. C., Millam, J. M., Iyengar, S. S., Tomasi, J., Barone, V., Mennucci, B., Cossi, M., Scalmani, G., Rega, N., Petersson, G. A., Nakatsuji, H., Hada, M., Ehara, M., Toyota, K., Fukuda, R., Hasegawa, J., Ishida, M., Nakajima, T., Honda, Y., Kitao, O., Nakai, H., Klene, M., Li, X., Knox, J. E., Hratchian, H. P., Cross, J. B.,Bakken, V., Adamo, C., Jaramillo, J., Gomperts, R., Stratmann, R. E., Yazyev, O., Austin, A. J., Cammi, R., Pomelli, C., Ochterski, J. W., Ayala, P. Y., Morokuma, K., Voth, G. A., Salvador, P., Dannenberg, J. J., Zakrzewski, V. G., Dapprich, S., Daniels, A. D., Strain, M. C., Farkas, O., Malick, D. K., Rabuck, A. D., Raghavachari, K., Foresman, J. B., Ortiz, J. V., Cui, Q.,Baboul, A. G., Clifford, S., Cioslowski, J., Stefanov, B. B., Liu, G., Liashenko, A., Piskorz, P.,Komaromi, I., Martin, R. L., Fox, D. J., Keith, T., Al-Laham, M. A., Peng, C. Y., Nanayakkara, A., Challacombe, M., Gill, P. M. W., Johnson, B., Chen, W., Wong, M. W., Gonzalez, C., & Pople, J. A. (2004). *Gaussian 03. Revision E.01.* Gaussian, Inc.: Wallingford, CT.
[31] Becke, A. D. (1992). *J. Chem. Phys.*, *97*, 9173.
[32] Becke, A. D. (1993). *J. Chem. Phys.*, *98*, 5648.
[33] Lee, C., Yang, W., & Parr, R. G. (1988). *Phys. Rev., B*, *37*, 785
[34] Snehalatha, M., Ravikumar, C., & Joe, I. H. (2009). *Solid State Sci.*, *11*, 1275.
[35] Dennington, II. R., Keith, T., & Millam, J. (2007). *GaussView, Version 4.1.2*. Semichem Inc., Shawnee Mission, KS.
[36] Pavlovic, G., Racane, L., Cicak, H., & Tralic-Kulenovic, V. (2009). *Dys. Pigments*, *83*, 354.
[37] Pajak, J., Rospenk, M., Ramaekers, R., Maes, G., Glowiak, T., & Sobczyk, L. (2001). *Chem. Phys,. 278*, 89.

[38] Marsman, A. V., Leussing, E. D., Zwikker, J. W., & Jenneskens, L. W. (1999). *Chem. Mater.*, *11*, 1484.
[39] Scrocco, E., & Tomasi, J. (1978). *Adv. Quant. Chem.*, *11*, 115.
[40] Roeges, N. P. G. (1994). *A Guide to Complete Interpretation of Infrared Spectra of Organic Structures*, Wiley, New York.
[41] Chaudhary, R. (2010). *S. J. Chem. Pharm. Res.*, *2*(4), 707.
[42] Özmen, Ü. Ö., & Olgun, G. (2008). *Spectrochimica Acta. Part A*, *70*, 641.
[43] Zülfikaroğlu, A., Taş, M., Batı, H., & Batı, B. (2003). *Synt. Reactivity İnorganic Metal-org. Chem.*, *33*(4), 625.
[44] Luque, F. J., Lopez, J. M., & Orozco, M. (2000). *Theor. Chem. Acc.*, *103*, 343.
[45] Okulik, N., & Jubert, A. H. (2005). *Internet Electron. J. Mol. Des.*, *4*, 17.
[46] Song, J., Zhao, P. S., & Zhang, W. G. (2010). *Bull. Korean. Chem. Soc.*, *1875*, 31.
[47] Fernando, M., & Claudio, O. A. (2005). *Int. J. Quant. Chem.*, *34*, 103.
[48] Olsenand, L. *et al.* (1995) *In: Modern Electronic Structure Theory*, World Science, River Edge, NJ.
[49] Fleming, I. (1976). *Frontier Orbitals and Organic Chemical Reactions*, Wiley: London.
[50] Weiqun, Z., Baolong, L., Yang, C., Yong, Z., & Xujie, L. L. Y. (2005). *J. Mol. Struct. Theochem.*, *117*, 715.